THEORETICAL AND EXPERIMENTAL STUDY OF JET VECTORING IN SUBSONIC FLOW FOR CIRCULAR NOZZLE

A.A.A. Asady[1], H.H.S, Alhafid[2]

[1,2]Baghdad University, College of Engineering,
Department of Mechanical Engineering
Baghdad, Iraq.

Email: [1]dralicit@yahoo.com, [2]Hussein.nu84@gmail.com

ABSTRACT: This paper presents theoretical and experimental investigations of thrust vectoring using co-flow method. The experimental investigation included a set of experiments carried out to demonstrate the ability to vector the exhaust flow in two axes (yawing and pitching angle) by secondary flow. A test rig was designed and constructed consisting of a circular duct in subsonic speed with four equals channels for secondary flow which represented the four directions of vectoring flow. And study the effect of various geometric variables on thrust vectoring angle. These included secondary slot height (h) and Coanda wall diameter (D) for a range of the mass flow ratio (ms/mp) ($0 \leq ms/mp \leq 0.07882$). Load measurements were obtained using four load cells. On the other hand, the theoretical investigation involved a 3D numerical solution by FLUENT Software for some of the experimental cases. The results showed that the thrust vectoring angle is proportional with the mass flow ratio and Coanda wall diameter, and inverse proportional with the secondary slot height. Three regions appear in the relationship curve between the mass flow ratio and thrust vectoring angle, that are "dead zone" region, control region and saturation region.

KEYWORDS: *Thrust Vectoring Angle; Jet Vectoring; Coanda Effect; Co-Flow; Mass Flow Ratio*

1.0 INTRODUCTION

The traditional aerodynamic control systems are limited by aerodynamic constraints because at all conditions in which aerodynamic forces are small, control is compromised or even lost. Such conditions are high angles of attack and low speed flight [1]. Thrust vectoring is redirect the proposal gasses from engine outlet nozzle of air vehicle to the desired direction that will turn the air vehicle around the center of mass in

opposite direction of the thrust. When the thrust is resolved into its components, this deflected thrust generates an additional component of thrust perpendicular to the centerline. This can have many benefits, the most common of these being reduced take-off and landing field length and/or improved maneuvering capabilities. In addition it reduces the cross section area of air vehicle and the radar signature (better stealth) as well as reduces the weight addition by aerodynamic control surface, which resulting in less fuel consumption.

Traditionally the thrust vectoring achieved by Mechanical thrust vectoring (MTV) is reflected by the path of proposed gasses from outlet nozzle engine or rocket by movable flaps and wings or by changing the direction of convergent nozzle powered by hydraulic or pneumatic actuators, MTV can divided into two types: 2-D thrust vectoring (pitching only) and 3-D thrust vectoring (yawing and pitching) and the vectoring angle achieved up to 20°. Generally, most fourth generation fighters and all fifth generation fighters used MTV. However, effective, these systems are complex and heavy, difficult to integrate, aerodynamically inefficient and expensive to maintain. With addition of the stealth requirements such as low observable shaping and IR suppression, the design and integration of an efficient MTV mechanical thrust vectoring system becomes more challenging [2].

Therefore new studies of thrust vectoring have achieved one of the most important studies, which is fluidic thrust vectoring. The majority of fluidic schemes developed for thrust vectoring use secondary flow injection to vector the main jet by using fluidic thrust control in place of thrust mechanical control. Important portions of nozzle hardware can be structurally integrated with the nonmoving airframe construction. This integration could allow the elimination of the mechanical actuators and kinematic structure, and may result in a significant decrease in nozzle weight, complexity, cost and the fast dynamic response of the fluidic devices. For these reasons, fluidic thrust vectoring FTV appeared as a very promising technology, and several techniques were developed.

Thrust vector control by secondary flow injection for rocket propulsion systems has been studied since the 1950's [23]. The Polaris missile utilized a secondary flow injection system in its axisymmetric circular exhaust nozzle for thrust vector control [3]. The fluidic thrust vectoring can be achieved by six techniques accomplished by continuous researches and experiments. Each method has been investigated both experimentally and numerically with different levels of success. The object of this work is co-flow thrust vectoring method that relies on a phenomenon known as the Coanda effect, which is the tendency of a

fluid jet initialized tangentially on a curved surface to remain attached to that surface. The effect is commonly seen in everyday jet flows such as a stream of water falling onto the convex side of a spoon. A second is the ability of a free jet to attach itself to a nearby surface [4].

Two methods of fluidic thrust vectoring are relay on Coanda effect. The first method is counter flow fluidic thrust vectoring which is based on the Coanda effect. Suction is applied to the plenum chamber in order to vector the primary flow according to the Coanda effect The asymmetric pressure loading generates a secondary reverse flowing stream at the wall of the suction coanda wall and nozzle flow is directed towards the low-pressure region. The schematic of the counter-flow FTV nozzle is shown in Figure 1. A reasonable vectoring angle can be achieved with careful design of the suction coanda wall but a limit must be imposed on the vectoring angle in order to prevent flow attachment. Throat area control is not possible with such systems. Although the secondary mass flow ratio is only about 1% of the primary flow, a viable vacuum source must still be sought. This would most likely be a turbo pump (driven by the engine). Unfortunately, counter-flow TV has some limitations such as suction supply source, stability with a highly over-expanded nozzle, hysteresis effects, thrust loss, and airframe integration [5].

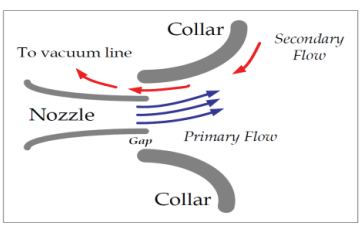

Figure 1: Schematic of counter flow thrust vector control geometry.

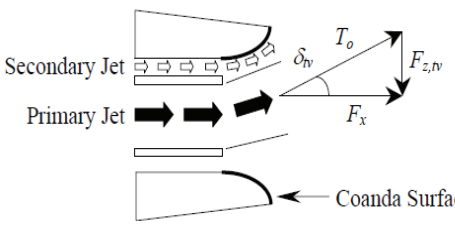

Figure 2: Co-Flow concept and forces schematic [1]

The co-flow FTV method relies on the Coanda effect phenomenon that has been mentioned earlier and will be investigated in this paper. When the secondary bleed air injects along the side of the primary jet nozzle outflow beside the coanda wall. The entrained air accelerates over the Coanda wall producing a local low-pressure region near the wall, which causes not only the injected flow but also the primary flow to move away from the normal thrust axis to the direction of the wall as shown in Figure 2. A co-flow FTV system has been developed for use on low observable unmanned air vehicles operating in the subsonic flight regime [6].

The four other methods of fluidic thrust vectoring are not relay on coanda effect and for supersonic speed that are Pulsed jet actuators (synthetic pules), Shock vector thrust vectoring, Sonic throat skewing (shifting) and combined vectoring methods [7].

FTV, however, introduces some new problems. The main problem is that FTV also needs a source of secondary air flow that leads to reduced engine thrust. Regardless of these problems, FTV still seems to have appealing options that improve the performance. The fact that FTV technology has not been employed in actual air vehicles indicates that it is still necessary to do more research and development on its effects and applications [8].

Theoretical and experimental investigations of thrust vectoring using co-flow method are discussed in the present work. The investigation includes a set of experiments carried out (i) to demonstrate the ability to vector the exhaust of an air machine in two axes (yawing and pitching angle) by secondary flow, and (ii) to study the effect of various geometric variables on thrust vectoring angle includes the variation of the secondary slot height (h), Coanda wall diameter (D) for wide ranges of the mass flow ratio. The theoretical investigation involves a 3D numerical solution of the problem by a commercial package Ansys Fluent 15.0. Each case tested in experimental investigation solved by the numerical solution.

2.0 NUMERICAL SIMULATION

Numerical simulations allow the analysis of a complex phenomenon without resorting to an expensive prototype and difficult experimental measurements, and in the case of this study it can predict the results for the secondary air mass flow rates that are beyond the maximum value that is achieved in the tests [9]. In order to analyze the flow field at the exit of primary and secondary duct, a solution of Navier-stokes equations and $\mathbf{k-\epsilon}$ turbulence model equations are required [10]. The numerical solution of the fluidic thrust vectoring, using governing partial differential equations in three dimensions are based on the conservation of mass, momentum and energy equations. In the present work, the mathematical model of the problem was solved numerically using a finite volume code, commercial package of FLUENT under ANSYS 15.0 software. This code was selected because of its unique capabilities to solve 3D problems and contains a wide range of turbulence models, after graphing the model by AUTOCAD 2013 and describing the mesh model by using ANSYS meshing 15.0. The CFD

simulations provided force data which were then compared to the experimental data obtained.

3.0 EXPERIMENTAL WORK

A photograph picture of the experimental set-up is shown in plate 1. An experimental rig was designed and constructed in the Heat Transfer Lab, at the Mechanical Engineering Department, University of Baghdad. The test section used in the present study consist of circular duct made of aluminum tube with the diameter of D=38 mm and length of L= 750 mm, utilizing different compatible secondary Coanda surfaces. A total of six rigs with different configurations were examined in order to investigate the effects of varying collar diameter D=20 mm, 40 mm and 60 mm (D/H= 0.52632, 1.052632, and 1.578947) and the effect of two different secondary slot heights h= 1 mm, and 2 mm (h/D= 0.02632, 0.0526) into the thrust-vectoring angle. These rings were made of aluminum with length of 30mm, outer diameter of D_o=73mm and inner diameter of D_i=(40mm,42mm) respectively for two slot height. A peripheral cylinder at the end of the duct with outer diameter 73 mm and inner diameter fit to the duct surface consist of four equal channels surrounding the circular duct at the exit with four inlets and four outlets with exit slot height 1mm and with inclined inner surface of channels. Ten different secondary air mass flows were tested for each ring in a specific main jet speed. By positioning the Coanda surface ring at the exit of the primary nozzle by two screws to the peripheral cylinder and introducing the secondary stream of co-flowing air, parallel to the Coanda surface, co-flow fluidic thrust vectoring can be obtained.

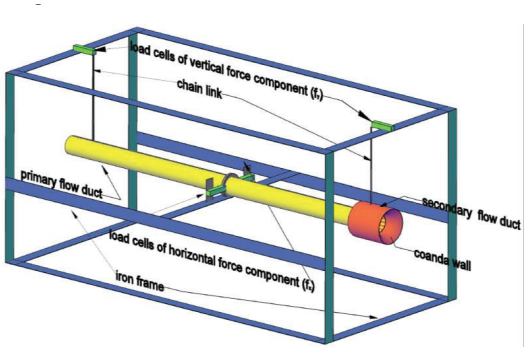

Figure 3: 3-D diagram of load cells location

The source of primary air flow is a centrifugal blower which has a constant volume rate equal to 11 m^3/min and pressure equal to 1.1 bars. It is connected to the duct by flexible rubber hose with gate valve to adjust the volume the exit speed and flow rate, and air compressor for secondary flow provide volume flow rate equal to (0.4) m^3/min, four load cells attached to the rig to measure the force component in x and y direction as shown in Figure (3. Several measurement devices that have been used are flow meter,

Anemometer and weight indicator. Other devices used to control the conditions of the experiment are regular valve to control the pressure in the secondary flow, DC power supply to provide a range of electricity voltage, electrical valve to control the direction of the thrust and four channels USB relay to control in the direction by a computer and programmed the valve. A smoke source is used to visualize the thrust.

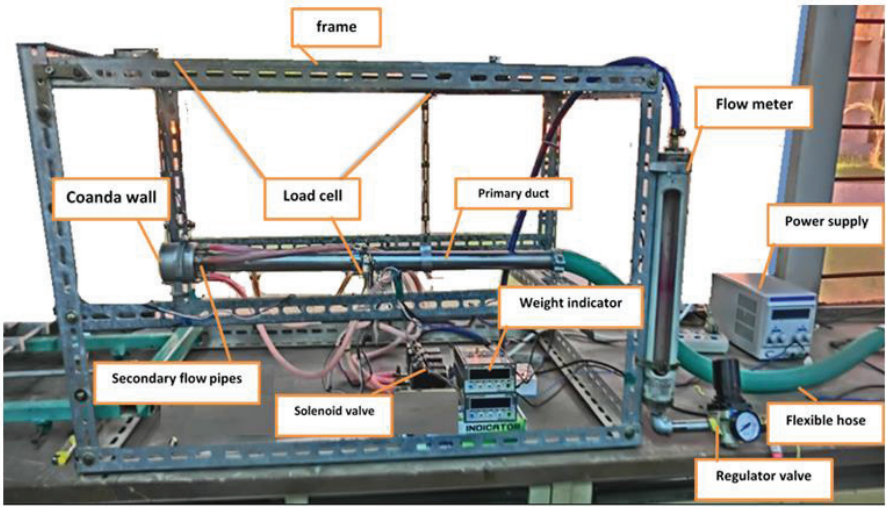

Plate 1: The experimental rig

4.0 RESULTS AND DISCUSSION

4.1. Experimental Results and Discussion

A series of tests were done in order to investigate the effect of various variables of geometry and condition of flow on thrust vectoring angle. These included secondary slot height (h), Coanda surface diameter (D) and mass flow ratio ($\dot{m}_{s/}\dot{m}_{p}$).

4.1.1 Varying Secondary Slot Height (h/d)

Figure 4 shows the relationship between the mass flow ratio $\dot{m}_{s/}\dot{m}_{p}$ (secondary flow rate/ primary flow rate) and the resultant thrust vectoring angle for different secondary gap heights and different Coanda wall diameters. Two secondary slot heights were examined h/d= (0.02632, 0.0526) and three Coanda wall diameters d/D= (0.5263, 1.052, 1.5789). The results show where the secondary mass flow ratio is increased, the thrust vectoring angle value increased to maximum value equal to (30.4) degree at h/d=0.02632 and d/D= 1.5789. It can be seen that when the secondary slot height increased, the values of the

thrust vectoring angle decreased to maximum value (27.84) degree for h/d = 0.0526 for the same coanda wall diameter d/D and mass flow ratio $\dot{m}_s/\dot{m}_p$as represented by the grey curve and green curve in Figure 4.

When the same secondary mass flow rate was tested in two different secondary duct slots height, the smaller slot height led to smaller exit cross section area that caused higher exit air velocity and lower pressure region generated at the exit of the slot causing more thrust vectoring angle for the primary airflow.

The result shows that there are three region forms in graphical representation between the secondary mass flow rate and vectoring angle, as shown in Figure 5. The first region shown when the low secondary flow rate a very small thrust vector angle is formed and it appears to be a 'dead zone' where no flow control can be done. After the 'dead zone', the Coanda effect governs and the curve arrives at the second region where a large increase in thrust vectoring angle can be achieved for relatively small increase in the secondary jet blowing rate. In this region, continuous control of the primary flow jet can be achieved. The third region is formed when there is no change in vectoring angle with increase of secondary flow rate as shown in Figure 4 at h/d=0.0263. This region is called saturation region.

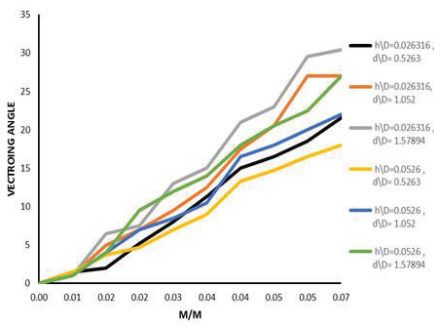

Figure 4: Relationship between m/m and the thrust vector for various h/d and D/d

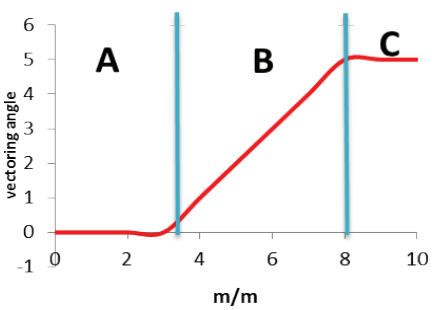

Figure 5: Trend line of the angle experimental results A – Dead zone, B – Control, C – Saturation

4.1.2 Varying Coanda Surface Diameter (D/d)

As shown in Figure 4, the relationship between the mass flow ratio ( ) and the resultant thrust vectoring angle for different Coanda wall diameters D/d= (0.5263, 1.0526, and 1.5789) are represented in black, red and gray curves respectively in Figure (4) at a constant secondary slot height ratio of h/H= 0.02632. When the mass flow ratio increases ,

the thrust vectoring angle increases, and as the Coanda wall diameter ratio is increased the slope of gradient of the curve increases and the 'dead zone' has been overcome. The diameter of the Coanda wall also determines the length of the 'dead zone' and hence where the active control region begins.

The results show that the secondary flow jet is more possible to separate from a Coanda wall with a small diameter and as a consequence the 'dead zone' will be prolonged over a wider range of the mass flow ratio values. Because the large diameter of the coanda wall provides a larger surface, the fluid is attached to it. The same results were obtained at a secondary slot height h/D=0.0526 for the three d/D tested as shown in orange , blue and green curves in Figure 4.

4.2 Numerical Results

A commercial package of ANSYS FLUENT15.0, 3D simulation has been used to solve the theoretical cases. Six cases have been studied, two varying secondary slots height at constant coanda wall and three varying coanda wall diameter with constant slot height. The results data are presented in contours of velocity magnitude, contours of static pressure and a vector of velocity magnitude. Using the figures directly reported from FLUENT for the resolved Fx and Fy on the coanda wall and circular ducts walls to obtain the thrust vectoring angle,

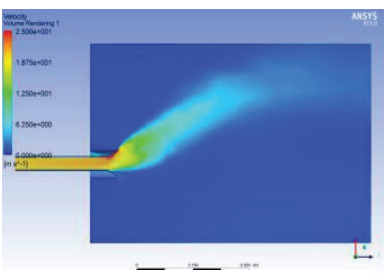

Figure 6: Velocity contour at $\dot{m}_s/\dot{m}_p$= 0.07882 and- D/d= 1.57894

Thrust vectoring angle = $\tan^{-1}\frac{Fy}{Fx}$

Figure 6 shows the velocity contour at $\dot{m}_s/\dot{m}_p$= 0.07882 and- D/d= 1.57894, h/d=0.0526 from ANSYS software result, where the red color represents the highest velocity and the blue color represents the lowest velocity. It shows the deflection in the flow direction at the exit of the duct.

4.2.1 Varying Secondary Slot Height (h/d)

Figure 7 shows the relationship between the mass flow ratio and the resultant thrust vectoring angle for different secondary slot heights and different Coanda wall diameters. The results data show that as the mass flow ratio is increased, the thrust vectoring angle increases and as

the secondary slot height increases, the values obtained for the thrust vectoring angle decreases for each mass flow ratio tested.

The same behavior in theoretical and experimental result gained but the values of the theoretical is higher.

4.2.2 *Varying Coanda Surface Diameter*

Figure 7 shows the relationship between the mass flow ratio ($\dot{m}_{s/}\dot{m}_{p}$) and the resultant thrust vectoring angle for the three Coanda walls diameters D/d= (0.5263, 1.0526, and 1.5789) at a constant secondary slot height ratio as shown in black, red and green curves in Figure 7. When the mass flow ration increased, the value of thrust vectoring increased, and as the Coanda wall diameter is increased the slope of the curve once, the 'dead zone' has been overcome. The diameter of the Coanda surface also determines the length of the 'dead zone' and hence where the active control region begins.

The same behaviors in theoretical and experimental results were gained but the values of the theoretical are higher; the dead zone is shorter in theoretical result and the saturation region appears earlier.

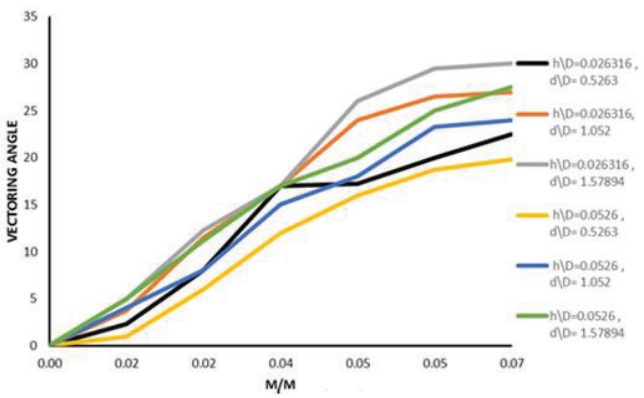

Figure 7: Relationship between m/m and the thrust vector angle for various h/d and D/d

4.3 *Smoke Flow Visualization*

A white smoke source was used in primary flow, applied on the primary flow blower inlet to visualize the airflow and the deflection that occur on it.

It can be seen in Plate 2 the visualization of a non-vectored primary jet where no secondary flow is applied (Vs = 0, ms/mp = 0), the flow

is not deflected from its axis. Plate 3 shows the Visualization of a vectored primary jet for Coanda surface diameters in the range of D/d= 1.5789 and ms/mp=0.07882 at constant secondary gap height ratio of h/d= 0.02632. It can be seen that the flow is deflected from its axis at vectoring angle 30.4^0.

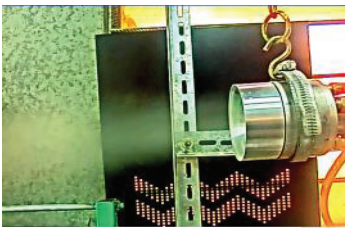

Plate 2: Non-vectored primary je

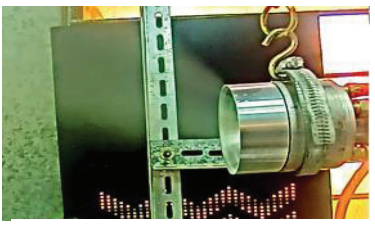

Plate 3: Vectored primary jet

4.4 Comparison Between Experimental and Theoretical Results

The experimental and numerical results have been compared with each other, as shown in Figure (8). It can be seen that both curves for theoretical and experimental results follow a similar trend. However, the extent of the 'dead zone' for the experimental work is more prolonged than that obtained in the theoretical work. The computational work has also highlighted both the control and saturation regions as seen previously in the experimental results. At mass flow ratio, the CFD investigation predicted greater thrust vectoring angle than those obtained during the experimental tests for approximately the same mass flow ratio. The percentage agreement between experimental and theoretical result is 92.08%.

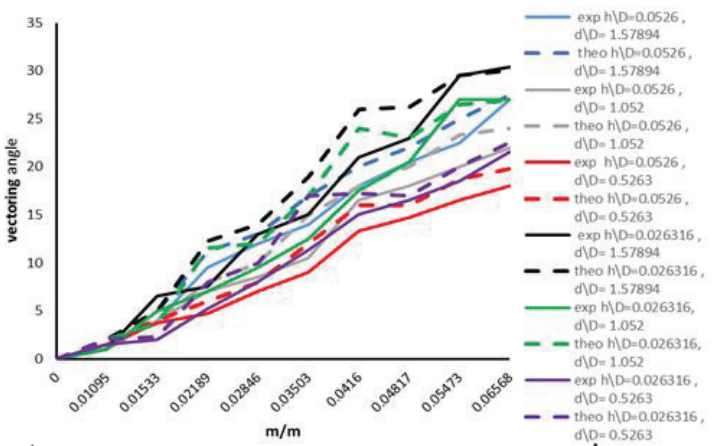

Figure 8: Relationship between m/m and the thrust vector angle for various h/d and D/d

4.5 *Comparison with Previous Work*

Verifying of the results obtained for the present study, a comparison was made with the results achieved by previous studies. The present results Thrust vectoring angle for varying secondary slot height and varying Coanda surface diameter shown in Figure 4 agree with the results of previous study [9] shown in Figure 9. The results show that as the secondary flow rate is increased, the resulting thrust vector angle increases. It can be seen that as the secondary slot height value increases, the values obtained for vectoring angle decreases accordingly at each mass flow ratio tested.

5.0 CONCLUSIONS

1. Both the theoretical and experimental results follow a similar trend. Three regions have been formed:, the first is the dead zone that appears at low (ms/mp) where no or small non-active thrust vectoring angle is obtained, the second region is the control zone where the active thrust vectoring control appears, the third region is the saturation region where there is no change in vectoring angle with increasing (ms/mp) due to physical limitation.

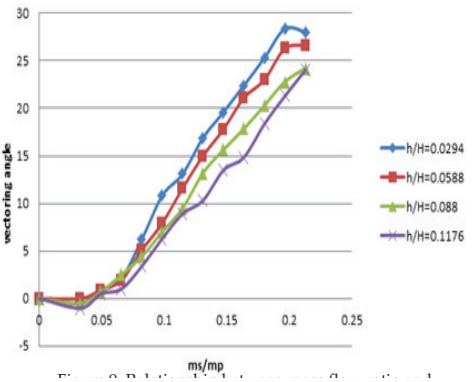

Figure 9: Relationship between mass flow ratio and thrust vectoring angle

2. Thrust vectoring angle is increased by increasing mass flow ratio (ms/mp).
3. The vectoring angle increases with increase of the coanda wall diameter at constant mass flow rate (ms/mp).
4. The length of the dead zone region depends on the coanda wall diameter; a prolonged dead zone appears at small coanda wall diameter and vice versa.
5. Thrust vectoring angle increases, as the secondary gap height decreases at constant mass flow rate (ms/mp).

6. The four directions active thrust vectoring control achieved by the circular nozzle designed in experimental rig simulates a subscale nozzle of small air-vehicle as shown in smoke visualization.

REFERENCES

[1] G. F. Schmid and P. J. Strykowski, Jet Attachment Behavior using Counterflow Thrust Vectoring, Minneapolis, University of Minnesota, 2000.

[2] T. M. Ragab and B. Elhadidi, Counter Flow Fluid Thrust Vector Applied to Small Business Jets, Military Technical College/ *Aerospace Sciences & AviationTechnology*, Cairo, Egypt 2009.

[3] M. S. Mason, W. J. Crowther, Fluidic Thrust Vectoring of Flow, University of Manchester, School of Engineering, Oxford Road, Manchester, 2002.

[4] A. Dustin,Axisymmetric Coanda-Assisted Vectoring Report, Utah State University, 2008.

[5] L.Li, Numerical and Experimental Studies of Fluidic Thrust Vectoring Mechanisms, Muroran Institute of Technology, Aerospace Engineering Division, 2011.

[6] E. Erinc, Thrust Vector Control by Secondary Injection, Middle East Technical University, 2006.

[7] B. L. Smith and A. Glezer, Jet Vectoring Using Synthetic Jets, Los Alamos National Laboratory, 2001.

[8] A. Sobester and A. J. Keane, Multi-objective Optimal Design of a Fluidic Thrust Vectoring Nozzle,Portsmouth, Virginia,University of Southampton, 2006.

[9] A. A. Mujahid, Thrust Vectoring of Fluid Jet Using Secondary Co-flow,University of Baghdad 2013.